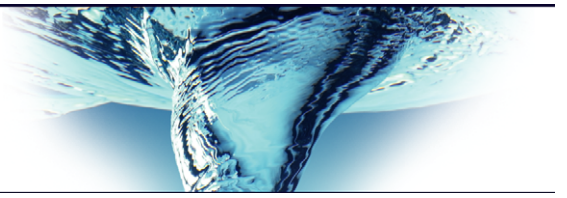
JFM RAPIDS
journals.cambridge.org/rapids



Bound-state formation in interfacial turbulence: direct numerical simulations and theory

M. Pradas[1], S. Kalliadasis[1,†], P.-K. Nguyen[2] and V. Bontozoglou[2]

[1]Department of Chemical Engineering, Imperial College London, London SW7 2AZ, UK
[2]Department of Mechanical Engineering, University of Thessaly, Pedion Areos, GR-38334 Volos, Greece

(Received 10 August 2012; revised 3 October 2012; accepted 11 October 2012)

We examine pulse interaction and bound-state formation in interfacial turbulence using the problem of a falling liquid film as a model system. We perform direct numerical simulations (DNSs) of the full Navier–Stokes equations and associated wall and free-surface boundary conditions and we examine both analytically and numerically a low-dimensional (LD) model for the film. For a two-pulse system, DNSs reveal the existence of very rich and complex pulse interactions, characterized by either overdamped, underdamped or self-sustained oscillating behaviours, all of them found to be in excellent agreement with LD results. Having demonstrated the reliability of the LD model for two-pulse systems/smaller domains, we use it to investigate larger domains with many interacting pulses, where DNSs are computationally expensive. We demonstrate that such systems are likely to be dominated by a self-sustained oscillatory dynamics.

Key words: instability, interfacial flows (free surface), thin films

1. Introduction

Understanding the dynamics and interaction of coherent structures is an active topic of fundamental research in nonlinear science. Coherent structures arise in many different physical and technological systems, often as a result of competition between energy production, internal dissipation–energy accumulation and nonlinearity. They play a crucial role in the so-called dissipative or interfacial turbulence (Manneville 1990), described by dissipative dynamical systems and characterized by the presence of a countable number of coherent structures in weak interaction. Interfacial turbulence is low-dimensional spatio-temporal chaos in the sense that, despite the apparent complexity, one can still identify localized coherent structures in what appears to be a randomly disturbed field. Moreover, these structures may exhibit some sort of

† Email address for correspondence: s.kalliadasis@imperial.ac.uk

 © Cambridge University Press 2013
doi:10.1017/jfm.2012.506

https://doi.org/10.1017/jfm.2012.506 Published online by Cambridge University Press

ordered and self-organized state, characterized by phenomena such as synchronization (Turaev, Vladimirov & Zelik 2012) or the formation of bound states (Duprat *et al.* 2009), i.e. groups of two or more structures behaving as a single object. In addition to a liquid film flowing down a planar vertical plane (Chang & Demekhin 2002; Kalliadasis *et al.* 2012), other well-known examples of interfacial turbulence in the context of fluid dynamics are thermal convection (Krishnamurti 1970), and the Faraday parametric instability (Miles & Henderson 1990), to name but a few.

In this study we address the question of bound-state formation in a liquid film flowing down a vertical wall. This is an example of a convectively unstable open-flow hydrodynamic system that exhibits a rich spatio-temporal dynamics and a sequence of wave instabilities and transitions that are generic to a large class of fluid dynamics and other nonlinear dissipative systems. It is well known that, for a falling film in the region of small-to-moderate values of the Reynolds number (defined typically as the ratio of the inlet flow rate to the kinematic viscosity), an initial small disturbance at the inlet is rapidly followed by a nearly spanwise-uniform wavy regime dominated by localized coherent structures, solitary waves, which are sufficiently stable and robust, and separated by relatively large portions of nearly flat films (Demekhin *et al.* 2007). These pulses consist of a nonlinear hump preceded by damping ripples at their front, and at sufficiently long distances from the inlet they continuously interact with each other, eventually forming bound states of two or more solitary waves travelling at the same speed. Previous studies on pulse dynamics and interaction include experimental ones (Liu, Paul & Gollub 1993), preliminary numerical investigations via direct numerical simulations (DNSs) of the full Navier–Stokes equations with the wall and free-surface boundary conditions (Vlachogiannis & Bontozoglou 2001; Malamataris, Vlachogiannis & Bontozoglou 2002), or both numerical and analytical studies via different low-dimensional (LD) models; see e.g. (Balmforth 1995; Chang, Demekhin & Kalaidin 1995; Pradas, Tseluiko & Kalliadasis 2011) – the last analytical study, in particular, resolved various details and subtleties overlooked in previous studies.

To date, there has not been a comparison between DNSs and LD model results, particularly on pulse interaction and bound-state formation. We present here the first such comparison as well as the first detailed, systematic and careful analysis of solitary-wave interactions by means of DNSs and both theory and numerical computations of an LD model, the 'second-order model' derived by Ruyer-Quil & Manneville (1998, 2000, 2002). Our analytical treatment of pulse interaction is based on the coherent-structure theory developed by Pradas *et al.* (2011) for a general system composed of N pulses. We apply these results to both two- and three-pulse systems. Our DNS study demonstrates the existence of bound states (doublets and triplets in the binary and three-pulse system, respectively), where the pulses appear to be separated by well-defined distances, which are found to be in excellent agreement with the theoretical predictions obtained from our coherent-structure theory. Unsteady DNSs of the binary system also show a very rich pulse dynamics, observing overdamped, underdamped, self-sustained oscillations or strong repulsions depending on the initial pulse separation length, which are also in excellent agreement with numerical solutions of the LD model (Pradas, Tseluiko & Kalliadasis 2012). Our findings thus demonstrate for the first time the reliability of using LD models as a simplified tool to study pulse interactions, especially for large domains where DNSs may become a formidable task. We also present new insights and results for a system composed of several pulses, observing that the initial relative location of the pulses may become a crucial factor for the final state of the system.

https://doi.org/10.1017/jfm.2012.506 Published online by Cambridge University Press

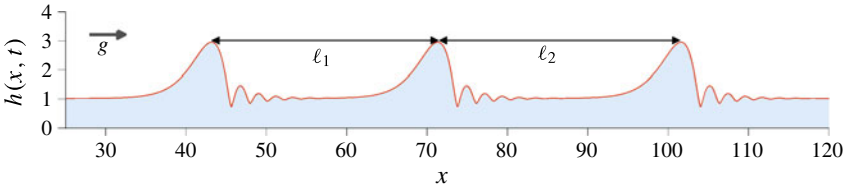


FIGURE 1. Example of solitary waves obtained by DNSs for $Re = 5.0$ ($\delta = 1.82$).

2. An example of dissipative turbulence: interfacial flows

Consider two-dimensional (2D) solitary waves in liquid films flowing down a vertical planar wall (see figure 1 for a sketch). The liquid is incompressible and Newtonian, with density ρ, dynamic viscosity μ, and surface tension σ. The free surface is taken as shear-free, i.e. the dynamic effect of a superposed gas phase is negligible. We take a Cartesian coordinate system, with the x-axis in the direction parallel to the wall and the y-axis outward-pointing normal to the wall. The primitive flow input is the volumetric flow rate per unit span, q, and the location of the free surface is denoted as $y = h(x, t)$. The Navier–Stokes equations governing the 2D flow are non-dimensionalized using as characteristic scales the Nusselt flat-film thickness, h_N, and mean velocity, $u_N = gh_N^2\rho/3\mu$, where g is the gravitational acceleration, while the characteristic time and pressure scales are given by $t_N = h_N/u_N$ and $p_N = \rho u_N^2$, respectively. A frame moving with the velocity c_0 of a single solitary pulse is introduced via the transformation, $x \to x - c_0 t$. The governing partial differential equations are hence formulated as follows:

$$\mathbb{M} := \boldsymbol{U}_t - c_0\boldsymbol{U}_x + \boldsymbol{U}\cdot\boldsymbol{\nabla}\boldsymbol{U} + \boldsymbol{\nabla}p - \frac{1}{Re}\nabla^2\boldsymbol{U} - \frac{3}{Re}\boldsymbol{g} = \boldsymbol{0}, \tag{2.1}$$

$$\mathbb{C} := \boldsymbol{\nabla}\cdot\boldsymbol{U} = 0, \tag{2.2}$$

where $\boldsymbol{U} = (u, v)^{\mathrm{T}}$ is the velocity vector in the laboratory frame and $\boldsymbol{g} = (1, 0)^{\mathrm{T}}$. The above equations are coupled to the kinematic equation for the free-surface evolution:

$$\mathbb{K} := h_t - c_0 h_x + uh_x - v = 0, \tag{2.3}$$

the no-slip and no-penetration boundary conditions on the wall, i.e. $u = v = 0$, and the dynamic boundary condition at the free surface, i.e. $\boldsymbol{n}\cdot\boldsymbol{T} = (\Delta p + 3^{1/3}\kappa Ka/Re^{5/3})\boldsymbol{n}$, where $\boldsymbol{T}$ is the stress tensor, $\boldsymbol{n}$ is the outward unit vector normal to the free surface and $\kappa = h_{xx}/(1 + h_x^2)^{3/2}$ is the surface curvature. The dimensionless parameters Re and Ka correspond to the Reynolds and Kapitza numbers, respectively, and they are defined as $Re = \rho u_N h_N/\mu$ and $Ka = \sigma(\rho/g\mu^4)^{1/3}$. Alternatively, two other dimensionless parameters, a reduced Reynolds number δ and a viscous dispersion number η, are often used in falling film studies (Kalliadasis *et al.* 2012), and are given as $\delta = (3Re)^{11/9}\,Ka^{-1/3}$ and $\eta = (3Re)^{4/9}\,Ka^{-2/3}$. In the results presented here, we use the so-called Shkadov scaling (Shkadov 1977), which involves the compression factor $\kappa = \eta^{-1/2}$ followed by the transformation $(x, y) \to (\kappa^{-1}x, y)$, $(u, v) \to (u, \kappa v)$ and $t \to \kappa^{-1}t$.

https://doi.org/10.1017/jfm.2012.506 Published online by Cambridge University Press

3. Direct numerical simulations: computational method

The computation of a single pulse travelling at constant speed c_0 is achieved by seeking stationary solutions of the governing equations (2.1), (2.2) and (2.3) written in the frame moving with velocity c_0, and they involve six field variables, namely u, v, p, h, c_0, and the pressure jump Δp of a reference point in the liquid to the (uniform) gas pressure. To close the system of equations, we provide two additional conditions by: (a) pinning the maximum of the hump at the middle of the flow domain, i.e. $h'(x = L/2) = 0$, where L is the system size (this eliminates a degeneracy without loss of generality); and (b) fixing the thickness of the undisturbed substrate far away from the main hump to $h(x = 0) = 1$. By using the Galerkin finite element method on a structured mesh, the system of governing equations is integrally weighted with bilinear $\Psi^i(\xi, \eta)$ $(i = 1, 9)$, biquadratic $\Phi^i(\xi, \eta)$ $(i = 1, 9)$ and quadratic basis functions $\Phi^i(\xi, \eta = 1)$ $(i = 1, 3)$, to produce, respectively, the residuals of the continuity, momentum and kinematic equations:

$$\iint_V \mathbb{M}\,\Phi^i(\xi, \eta)\,\mathrm{d}V = 0, \quad \iint_V \mathbb{C}\,\Psi^i(\xi, \eta)\,\mathrm{d}V = 0, \quad \int_S \mathbb{K}\,\Phi^i(\xi, \eta = 1)\,\mathrm{d}S = 0, \quad (3.1)$$

where V and S represent volume domain and surface boundary, respectively. The flow field variables consisting of u, v, p and h are also interpolated from nodal unknowns using the bases: $\boldsymbol{U} = \sum_{i=1,9} \boldsymbol{U}_i \Phi^i(\xi, \eta)$, $p = \sum_{i=1,4} p_i \Psi^i(\xi, \eta)$ and $h = \sum_{i=1,3} h_i \Phi^i(\xi, \eta = 1)$. The elementwise integration of (3.1) is made by the nine-, four- and three-point Gaussian quadratures, respectively. The time integration is based on a Crank–Nicolson scheme. The resulting system of algebraic equations is solved by a Newton–Raphson iterative algorithm, coupled with a frontal technique.

Systematic numerical integrations of a single-pulse system show that the wave speed and pulse height converge to the infinite-domain solution (up to a 10^{-5} tolerance) for spatial periodic domains of $L \geqslant 60$. It is important to remark that such a rapid numerical convergence is mainly due to the exponentially fast decay of both the front and back pulse tails. Doublet converged solutions are then obtained as follows. First, two of the single-pulse converged solutions are assembled next to each other along the streamwise direction. By removing a certain number of elements in the film region joining the two pulses, this initial structure is modified until it satisfies the equations, but with a small error due to a discontinuity in the joining zone. Despite this small error, initial bound-state guesses with very closely spaced pulses can be successfully constructed – the use, for example, of a naive superposition of two single-pulse solutions would lead to unacceptably high film thickness in between. To guarantee then size independence, computations are carried out by taking periodic domains up to $L = 140$. As we show in § 5, DNS results are found to be in excellent agreement with asymptotic (infinite-domain) theoretical predictions, hence pointing out the good numerical convergence of the method. Likewise, the construction of an initial guess for a bound-state triplet can be obtained by joining a numerically converged doublet with a single pulse. The location of the single pulse is then fixed while the other two are left to relax to equilibrium positions. It should be noted, however, that convergence to bound states is numerically more tedious for triplets than for doublets, and especially for relatively high flow rates.

4. Low-dimensional model and coherent-structure theory

The analytical study of the interface dynamics is carried out by making use of an integral boundary layer LD model, which is much easier to treat than the primitive

https://doi.org/10.1017/jfm.2012.506 Published online by Cambridge University Press

governing equations, but also captures the main physical mechanisms and elementary dynamic characteristics of the full problem. The LD model is chosen as the two-field second-order model derived by Ruyer-Quil & Manneville (1998, 2000, 2002), which describes the evolution of both the interface thickness $h(x,t)$ and local flow rate $q(x,t)$:

$$\delta q_t = \frac{5}{6}h - \frac{5}{2}\frac{q}{h^2} + \delta\left(\frac{9}{7}\frac{q^2}{h^2}h_x - \frac{17}{7}\frac{q}{h}q_x\right) + \frac{5}{6}hh_{xxx} + \eta\left[4\frac{q}{h^2}(h_x)^2 - \frac{9}{2h}q_xh_x - 6\frac{q}{h}h_{xx} + \frac{9}{2}q_{xx}\right], \tag{4.1}$$

$$h_t = -q_x. \tag{4.2}$$

The above model was obtained by combining the long-wave expansion up to second order with a weighted residual technique based on a Galerkin projection in which the velocity field is expanded onto a basis with polynomial test functions (Ruyer-Quil & Manneville 1998, 2000, 2002) – this formulation was extended to three dimensions in the study by Scheid, Ruyer-Quil & Manneville (2006), which also included a detailed theoretical investigation of falling film dynamics. It is worth mentioning that this model contains the second-order viscous dispersion terms (those gathered in the second line of (4.1)), which affect both the amplitude and frequency of the capillary ripples of the pulses (Ruyer-Quil & Manneville 2000) and also corrects the shortcomings of the first-order model obtained by Shkadov (1967), with the principal one being an erroneous prediction of the instability onset. Also, as was demonstrated by Pradas *et al.* (2011), such second-order terms play an important role in the pulse interactions precisely because they affect both the amplitude and frequency of the capillary ripples of the pulses.

Bound-state formation and pulse interactions in model (4.1) are studied by making use of a coherent-structure theory that has been recently developed by Pradas *et al.* (2011) for a system composed of N pulses weakly interacting through their tails. For the sake of clarity, we recall here the main points of this theory; the reader is referred to the above study for details. The solution was assumed to be a superposition of N pulses and a small correction function, i.e. $\boldsymbol{\Phi} = \boldsymbol{\Phi}_N + \sum_i \boldsymbol{\Phi}_i + \hat{\boldsymbol{\Omega}}(x,t)$, for $i = 1,\ldots,N$ written in vectorial form, where $\boldsymbol{\Phi} = (q \quad h)^{\mathrm{T}}$, $\boldsymbol{\Phi}_N = (q_N \quad h_N)^{\mathrm{T}}$ corresponds to the Nusselt flat-film solution, $\boldsymbol{\Phi}_i = \boldsymbol{\Phi}_0(x - x_i(t))$ with $\boldsymbol{\Phi}_0 = (q_0 \quad h_0)^{\mathrm{T}}$ and $x_i(t)$ is the stationary solution and location of each pulse, respectively; and $\hat{\boldsymbol{\Omega}}$ is the small correction function. Weak interaction was considered by assuming large pulse separation lengths, i.e. $\ell_i \equiv x_{i+1} - x_i \gg 1$. By defining a small parameter $\varepsilon = \exp(-\min_i\{\ell_i\})$ and assuming pulse velocities $\dot{x}_i(t)$ and $\hat{\boldsymbol{\Omega}}$ to be of $O(\varepsilon)$, it was possible to obtain asymptotically the following dynamical linear equation for the correction function in the vicinity of each pulse:

$$\hat{\boldsymbol{\Omega}}_t - \dot{x}_i(t)\,\boldsymbol{\Phi}_{ix} = \boldsymbol{\mathcal{L}}_i\hat{\boldsymbol{\Omega}} + \boldsymbol{\mathcal{J}}_i\boldsymbol{\Phi}_{i-1} + \boldsymbol{\mathcal{J}}_i\boldsymbol{\Phi}_{i+1}, \tag{4.3}$$

where $\boldsymbol{\mathcal{L}}_i$ and $\boldsymbol{\mathcal{J}}_i$ are linear differential operators. By rigorously scrutinizing the spectrum of $\boldsymbol{\mathcal{L}}_i$ and expanding $\hat{\boldsymbol{\Omega}}$ in terms of its dominant eigenfunctions, which turn out to be those belonging to its null space, it was possible to project the above equation onto the dominant modes to obtain the following dynamical system:

$$\dot{x}_i(t) = \alpha_i S_1(x_{i+1} - x_i) + \beta_i S_2(x_i - x_{i-1}), \tag{4.4}$$

https://doi.org/10.1017/jfm.2012.506 Published online by Cambridge University Press

with $\alpha_i = \beta_i = 1$ for $i = 2, \ldots, N-1$, $\alpha_1 = \beta_N = 1$ and $\alpha_N = \beta_1 = 0$. The functions S_1 and S_2 are given by the projection of the terms $\boldsymbol{\mathcal{J}}_i \boldsymbol{\Phi}_{i+1}$ and $\boldsymbol{\mathcal{J}}_i \boldsymbol{\Phi}_{i-1}$, respectively, to the null space of $\boldsymbol{\mathcal{L}}_i$.

5. Results

5.1. *Two-pulse system: doublet formation*

We use water as the working liquid throughout the whole study, with $\mu = 10^{-3}$ kg m^{-1} s, $\rho = 1000$ kg m^{-3} and $\sigma = 72.01$ mN m^{-1}, giving a Kapitza number of $Ka = 3364$. We first focus on a two-pulse system, and consider two cases of flow rates corresponding to $\delta = 0.98$ ($Re = 3$) and $\delta = 1.82$ ($Re = 5$).

For a system composed of two pulses, the dynamical system (4.4) reduces to $\dot{x}_1(t) = S_1(x_2 - x_1)$ and $\dot{x}_2(t) = S_2(x_2 - x_1)$, which we rewrite as

$$\dot{\ell} = -\partial_\ell V_c(\ell), \tag{5.1}$$

for $\ell = x_2 - x_1$, where $V_c(\ell) \equiv \int_\ell [S_1(\ell) - S_2(\ell)]$ with $V_c(\ell \to \infty) = 0$. As shown by Pradas *et al.* (2012), this potential function can be physically related to the net capillary force between both pulses, and its local maxima and minima correspond to unstable and stable doublets, respectively. In particular, by assuming the interface profile between both pulses to be $h(x) = 1 + A\cos(\beta x + \theta)\exp(-m_1 x) + B\exp[-m_2(\ell - x)]$, where β, m_1 and m_2 represent the frequency of the capillary ripples and decay of the tails, respectively, θ a shift phase, and A and B arbitrary constants, one obtains

$$V_c(\ell) = m_2 B \mathrm{e}^{-m_2 \ell} - A m_1 \mathrm{e}^{-m_1 \ell}[\beta \sin(\beta\ell + \theta) + m_1 \cos(\beta\ell + \theta)], \tag{5.2}$$

for sufficiently large separation lengths. Alternatively, S_1 and S_2 are also given as

$$S_1(\ell) = -B m_2^2 \mathrm{e}^{-m_2 \ell}, \quad S_2(\ell) = A\mathrm{e}^{-m_1 \ell}[(\beta^2 - m_1^2)\cos(\beta\ell + \theta) - 2m_1\beta \sin(\beta\ell + \theta)]. \tag{5.3}$$

Figure 2(*a*,*b*) shows the potential function for $\delta = 0.98$ and 1.82, respectively, obtained from the coherent-structure theory, i.e. by solving the corresponding eigenfunctions of the linearized operator and computing S_1 and S_2 in (5.1). From a data fit to (5.2) we obtain the numerical values of $m_1 = 0.28$, $m_2 = 1.44$, $\theta = 0.57$, $\beta = 0.92$, and $m_1 = 0.31$, $m_2 = 3.49$, $\theta = -11.68$, $\beta = 3.0$ for $\delta = 0.98$ and 1.82, respectively.

On the other hand, DNS steady-state solutions show the existence of a countable number of stable and unstable bound states for both flow rate cases (see figure 2*a*,*b*). We observe an excellent agreement at intermediate and large separation distances, and, as expected, a deviation between theory and DNSs occurs at the shortest separation distances, where strong interactions between pulses start to play a prominent role. The dynamics of both pulses has been studied by computing unsteady DNSs for $\delta = 1.82$ and by choosing different initial separation lengths ℓ_0. At large initial distances, it is seen that both pulses approach monotonically (either attracting or repelling each other) to the closest stable bound state (see figure 2*d*). At moderate initial distances, we observe both pulses to repel and attract each other in an underdamped oscillatory manner, eventually reaching a constant separation length which corresponds to one of the stable doublets predicted theoretically (see the initial distance of $\ell_0 = 28.17$ in figure 2*c*).

As we decrease the initial separation length, however, our DNS results show the emergence of a self-sustained oscillatory state, where the pulse separation length oscillates now at constant frequency and non-decaying amplitude around a stable

https://doi.org/10.1017/jfm.2012.506 Published online by Cambridge University Press

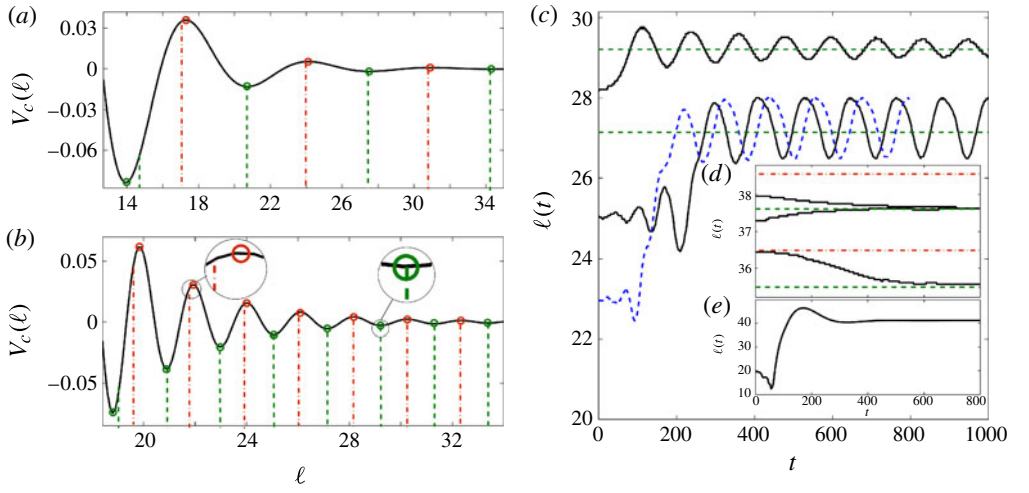


FIGURE 2. Potential function for (*a*) $\delta = 0.98$ and (*b*) $\delta = 1.82$. Circles denote the exact position of the local minima and maxima. Dashed and dot-dashed lines mark the DNS solutions of the stable and unstable doublets, respectively. (*c–e*) DNS dynamic evolution of doublets for $\delta = 1.82$ obtained by choosing different initial separation lengths. Dashed and dot-dashed horizontal lines denote theoretical stable and unstable doublets, respectively.

doublet, which is predicted by the theory (see the initial distance of $\ell_0 = 25.06$ in figure 2*c*). It should be noted that such an oscillatory behaviour is clearly harmonic, demonstrating a periodic attracting–repelling alternation under the gravity forcing. This behaviour is coupled to the mass exchange between pulses: the growing pulse accelerates and the shrinking pulse decelerates, and their overshoot leads to an oscillation. The amplitude of the separation length is then confined between two neighbouring unstable positions.

Figure 2(*c*) also reflects the complex nature of pulse interactions. First, we note that different initial separation lengths ranging in $\ell_0 = [22, 28]$ lead to the same oscillatory behaviour around $\ell = 27.20$. This means that the stable doublets, which were found at distances below $\ell \sim 27$ in steady solutions (cf. figure 2*b*), turn out to be unstable when we consider unsteady computations. Therefore, any ℓ_0 chosen in the range of $\ell \sim [22, 28]$ is attracted towards the oscillatory state. Also, we observe that both the amplitude and frequency of the final oscillatory state are independent of the initial condition; for example, we find that starting with either $\ell_0 = 27.63$, which is slightly perturbed from the stable state located around 27.20, or a strongly perturbed initial separation of $\ell_0 = 22.93$, leads to a similar frequency and amplitude (see dashed curve in figure 2*c*).

Finally, we also observe that for even smaller initial separation lengths ($\ell < 22$, cf. figure 2*e*), there is an initial strong repulsive interaction that causes both pulses to rapidly repel each other, exhibiting a monotonic growth until the pulses get locked into a stable bound state located at much larger distances, including a slight attraction and then an overshoot correction. From a physical point of view, this behaviour may be qualitatively explained by considering that, at short separations, pulse interactions occur not only via the tails (weak theory), but also between the main humps and capillary ripples, giving rise to a more complex interaction. Therefore, the oscillatory

https://doi.org/10.1017/jfm.2012.506 Published online by Cambridge University Press

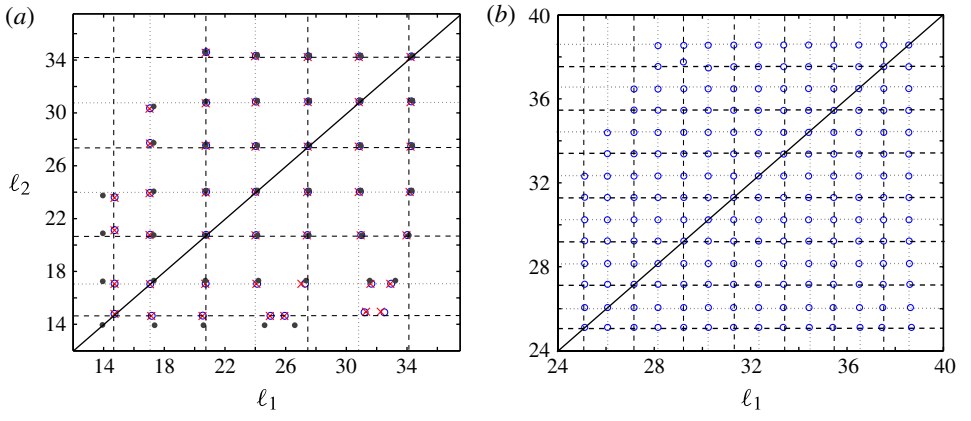


FIGURE 3. Numerically found steady triplets (ℓ_1, ℓ_2) for: (a) $\delta = 0.98$ with DNSs (crosses), LD model (circles) and coherent-structure theory of equation (5.4) (solid points); (b) $\delta = 1.82$. Dashed and dotted lines mark stable and unstable doublet positions, respectively, obtained from (5.1).

solutions found around the stable bound state $\ell = 27.12$ demarcate the transition from, on the one hand, a monotonic approach to stable equilibrium at much larger separations, and, on the other, strong repulsive growth at much shorter separations. In this sense, such oscillatory states may be viewed as metastable states, which could tentatively be attributed to a narrow attractor of film flow dynamics. It is important to remark that all the different dynamic behaviours observed with DNSs are in excellent agreement with numerical computations of the second-order model (Pradas *et al.* 2012). Note also that, although weak-interaction theory is not valid to describe such a complex dynamics observed at these short separation distances (i.e. oscillations or strong repulsions), our results show that it is indeed capable of theoretically predicting stable and unstable bound-state formation.

5.2. *Three-pulse system: triplet formation*

For a system of three pulses (4.4) reduce to $\dot{x}_1(t) = S_1(x_2 - x_1)$, $\dot{x}_2(t) = S_1(x_3 - x_2) + S_2(x_2 - x_1)$ and $\dot{x}_3(t) = S_2(x_3 - x_2)$, which we rewrite as

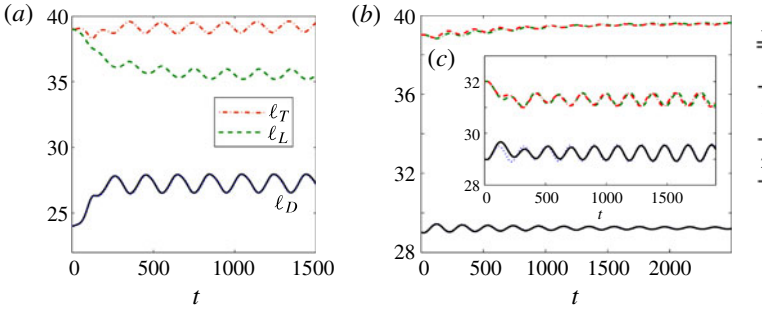
$$\dot{\ell}_1 = -\partial_{\ell_1} V_c(\ell_1) + S_1(\ell_2), \tag{5.4a}$$

$$\dot{\ell}_2 = -\partial_{\ell_2} V_c(\ell_2) - S_2(\ell_1), \tag{5.4b}$$

for $\ell_1 = x_2 - x_1$ and $\ell_2 = x_3 - x_2$, where $V_c(\ell)$ is given as in (5.1).

Numerically steady triplets (ℓ_1, ℓ_2) obtained with DNSs, the second-order model and the dynamical system of (5.4) for $\delta = 0.98$ are shown in figure 3(a). As before, we find very good agreement between the numerical results, especially for separations $\ell > 16$. As expected, for shorter distances, however, theoretically predicted triplets (solid points) deviate from DNSs and LD computations. It is interesting to note that having a third pulse in the system may affect the distances at which bound states are formed as compared to the doublet system. Points along the diagonal indicate that, if the leading and trailing pulses are placed symmetrically with respect to the middle one, the equilibrium separation distances are similar to those obtained in a binary system. However, when the leading and trailing pulses are placed asymmetrically (points off

https://doi.org/10.1017/jfm.2012.506 Published online by Cambridge University Press



ℓ_0	Doublet	Triplet
36	Over-damped	Over-damped
29	Under-damped	Self-sustained oscillations
27	Self-sustained oscillations	Self-sustained oscillations

FIGURE 4. Dynamic evolution of triplets for $\delta = 1.82$ by choosing different initial separation lengths: (*a*) $(\ell_D, \ell_L) = (24, 39)$ and $(\ell_T, \ell_D) = (39, 24)$; (*b*) $(\ell_D, \ell_L) = (29, 39)$ and $(\ell_T, \ell_D) = (39, 29)$; and (*c*) $(\ell_D, \ell_L) = (29, 32)$ and $(\ell_T, \ell_D) = (32, 29)$. Solid and dotted lines correspond to ℓ_D for the (ℓ_D, ℓ_L) and (ℓ_T, ℓ_D) configurations, respectively; and dashed and dot-dashed lines correspond to ℓ_L and ℓ_T, respectively. The table on the right shows dynamic states for doublets with $\ell(0) = \ell_0$ and triplets with $\ell_1(0) = \ell_2(0) = \ell_0$.

the diagonal), we observe that the pair of pulses with the shortest separation length equilibrates with the remaining pulse at separation lengths that deviate considerably from the binary system, especially at short distances (see for $\ell_2 \simeq 15$ and $\ell_1 > 20$). It is also important to note that these results depend on whether the pair with shortest distance is located in front of or behind the remaining pulse. In particular, we remark that no steady-state solutions were found at the top left corner of the panel. This effect is also observed at higher flow rates ($\delta = 1.82$, cf. figure 3*b*). It should also be emphasized that DNSs for triplet systems start to become computationally expensive, especially at high flow rates, as the high-amplitude wave and ripples make initial guesses more difficult to converge to steady-state solutions. The numerical results of figures 3(*b*) and 4 are hence obtained with the second-order model only. We note that the excellent agreement observed in the doublet and triplet cases indicates that the LD formulation is indeed a good alternative to full Navier–Stokes for the study of pulse interactions.

Figure 4 shows the dynamic behaviour of the triplet system for $\delta = 1.82$. As observed for the binary system, pulse dynamics may become quite complex. For clarity, if $\ell_1 \leqslant \ell_2$, we denote $\ell_D = \ell_1$ and $\ell_L = \ell_2$ (leading pulse), or otherwise $\ell_D = \ell_2$ and $\ell_T = \ell_1$ (trailing pulse) if $\ell_1 > \ell_2$. First, we observe that, for a short initial separation distance of $\ell_D = 24$, the pair evolves into the self-sustained oscillatory state located around $\ell_D = 27.2$, which corresponds to the same dynamic behaviour obtained from DNSs for a binary system (cf. figure 2*c*). The final state of the remaining pulse, however, depends on whether the pulse is at the leading or trailing position. This is actually consistent with the steady-state results of figure 3(*b*), where no stable solutions were observed at the top left corner. Indeed, for the initial case of $(\ell_D, \ell_L) = (24, 39)$, the nearest observable stable state is located at $(27.2, 35.5)$ and the leading pulse separation length hence decays (see figure 4*a*). On the other hand, for the reversed case of $(\ell_T, \ell_D) = (39, 24)$, the nearest observable stable bound state happens to be now at $(39.4, 27.2)$, and the trailing pulse separation length ℓ_T increases. We note that the observation of such asymmetric behaviour depends in turn on the initial separation length of ℓ_D. Figure 4(*b*) shows the time evolution for initial

https://doi.org/10.1017/jfm.2012.506 Published online by Cambridge University Press

configurations of $(\ell_D, \ell_L) = (29, 39)$ and $(\ell_T, \ell_D) = (39, 29)$, obtaining in both cases the same final state. Note also that the dynamics of the pair of pulses separated by ℓ_D is characterized by damped oscillations, as observed with DNSs in figure 2(*c*).

Finally, we find that the dynamics of the pair of pulses separated by ℓ_D also depends on the distance of the remaining pulse. For example, figure 4(*c*) shows that, when the third pulse (either trailing or leading) is placed sufficiently close to the other pair, the final state evolves to the self-sustained oscillatory state. This means that self-sustained oscillatory dynamics is more likely to be observed in systems composed of several pulses that are sufficiently close to each other (see the movie '7pulses_Re_5.mov' in the supplementary material (available at journals.cambridge.org/flm) for a case of seven pulses initially separated by $\ell_0 = 29$), where we can also observe how both configurations $(\ell_1, \ell_2) = (\ell_D, \ell_L)$ and $(\ell_1, \ell_2) = (\ell_T, \ell_D)$ are continuously switching over. Figure 4 also depicts a table describing all possible doublet and triplet dynamic states.

6. Conclusions

We have performed a detailed and systematic investigation of pulse interactions in falling films via both DNS and analysis–numerical simulations of the LD model derived by Ruyer-Quil & Manneville (1998, 2000, 2002). The analysis of the model was done using elements from the coherent-structure theory developed in Pradas *et al.* (2011) for a system of N pulses; the cases of two and three interacting pulses were examined here.

In a binary system, our DNSs showed bound-state (doublet) formation with a complex dynamics that strongly depends on the initial conditions. For large initial separation lengths, both pulses may exponentially attract or repel each other, eventually approaching theoretically predicted stable doublets. For moderate separation lengths, the oscillatory behaviour observed at short times is eventually damped. When both pulses are initially placed at sufficiently close distances, a self-sustained state where both pulses oscillate at constant frequency emerges. Excellent agreement between theory and DNSs was found.

The LD model and coherent-structure theory are therefore very good tools for the study of pulse interactions and particularly useful for large domains with several pulses where DNSs require long and tedious computations. In a three-pulse system, for example, we found that DNSs start to be computationally expensive at high flow rates ($\delta = 1.82$). At lower flow rates, we were still able to study steady-state solutions of triplets, observing that the presence of a third pulse affects the bound-state separation distance of the other two pulses, and is reflected asymmetrically due to the different interactions between the front (ripples) and back (tail) of the pulse. This was also obtained with LD results at both low and high flow rates. In addition, unsteady LD computations revealed that self-sustained oscillations are more likely to happen in systems of many interacting pulses. This is consistent with the numerical results of Pradas *et al.* (2011) using random initial conditions for long domains, the statistical analysis of which indicates that pulse separation may exhibit a broad distribution around specific mean distances.

Acknowledgements

We acknowledge financial support from EU-FP7 ITN Multiflow and ERC Advanced Grant No. 247031. We are grateful to Dmitri Tseluiko for stimulating discussions on coherent structures.

https://doi.org/10.1017/jfm.2012.506 Published online by Cambridge University Press

Supplementary movies

Supplementary movies are available at journals.cambridge.org/flm.

References

BALMFORTH, N. J. 1995 Solitary waves and homoclinic orbits. *Annu. Rev. Fluid Mech.* **27**, 335–373.

CHANG, H.-C. & DEMEKHIN, E. 2002 *Complex Wave Dynamics on Thin Films*. Springer.

CHANG, H.-C., DEMEKHIN, E. & KALAIDIN, E. 1995 Interaction dynamics of solitary waves on a falling film. *J. Fluid Mech.* **294**, 123–154.

DEMEKHIN, E. A., KALAIDIN, E. N., KALLIADASIS, S. & VLASKIN, S. YU. 2007 Three-dimensional localized coherent structures of surface turbulence. I. Scenarios of two-dimensional–three-dimensional transition. *Phys. Fluids* **19**, 114103.

DUPRAT, C., GIORGIUTTI-DAUPHINÉ, F., TSELUIKO, D., SAPRYKIN, S. & KALLIADASIS, S. 2009 Liquid film coating a fiber as a model system for the formation of bound states in active dispersive–dissipative nonlinear media. *Phys. Rev. Lett.* **103**, 234501.

KALLIADASIS, S., RUYER-QUIL, C., SCHEID, B. & VELARDE, M. G. 2012 *Falling Liquid Films*. *Springer Series on Applied Mathematical Sciences*, vol. 176 Springer.

KRISHNAMURTI, R. 1970 On the transition to turbulent convection. Part 1. The transition from two- to three-dimensional flow. *J. Fluid Mech.* **42**, 295–307.

LIU, J., PAUL, J. D. & GOLLUB, J. P. 1993 Measurements of the primary instabilities of film flows. *J. Fluid Mech.* **250**, 69–101.

MALAMATARIS, N. A., VLACHOGIANNIS, M. & BONTOZOGLOU, V. 2002 Solitary waves on inclined films: flow structure and binary interactions. *Phys. Fluids* **14**, 1082–1094.

MANNEVILLE, P. 1990 *Dissipative Structure and Weak Turbulence*. Academic Press.

MILES, J. & HENDERSON, D. 1990 Parametrically forced surface waves. *Annu. Rev. Fluid Mech.* **22**, 143.

PRADAS, M., TSELUIKO, D. & KALLIADASIS, S. 2011 Rigorous coherent-structure theory for falling liquid films: Viscous dispersion effects on bound-state formation and self-organization. *Phys. Fluids* **23**, 044104.

PRADAS, M., KALLIADASIS, S. & TSELUIKO, D. 2012 Binary interactions of solitary pulses in falling liquid films. *IMA J. Appl. Maths* **77**, 408–419.

RUYER-QUIL, C. & MANNEVILLE, P. 1998 Modelling film flows down inclined planes. *Eur. Phys. J. B* **6**, 277–292.

RUYER-QUIL, C. & MANNEVILLE, P. 2000 Improved modelling of flows down inclined planes. *Eur. Phys. J. B* **15**, 357–369.

RUYER-QUIL, C. & MANNEVILLE, P. 2002 Further accuracy and convergence results on the modeling of flows down inclined planes by weighted-residual approximations. *Phys. Fluids* **14**, 170–183.

SCHEID, B., RUYER-QUIL, C. & MANNEVILLE, P. 2006 Wave patterns in film flows: modelling and three-dimensional waves. *J. Fluid Mech.* **562**, 183–222.

SHKADOV, V. YA. 1967 Wave modes in the flow of thin layer of a viscous liquid under the action of gravity. *Izv. Akad. Nauk SSSR Mekh. Zhidk. Gaza* **1967** (1), 43–50.

SHKADOV, V. YA. 1977 Solitary waves in a layer of viscous liquid. *Izv. Akad. Nauk SSSR Mekh. Zhidk. Gaza* **1977** (1), 63–66.

TURAEV, D., VLADIMIROV, A. G. & ZELIK, S. 2012 Long-range interactions and synchronization of oscillating dissipative solitons. *Phys. Rev. Lett.* **108**, 263906.

VLACHOGIANNIS, M. & BONTOZOGLOU, V. 2001 Observations of solitary wave dynamics of film flows. *J. Fluid Mech.* **435**, 191–215.

https://doi.org/10.1017/jfm.2012.506 Published online by Cambridge University Press